

Article

Nonlinearity of Microwave Electric Field Coupled Rydberg Electromagnetically Induced Transparency and Autler-Townes Splitting

Liping Hao ¹, Yongmei Xue ¹, Jiabei Fan ¹, Yuechun Jiao ^{1,2}, Jianming Zhao ^{1,2,*}  and Suotang Jia ^{1,2}

¹ State Key Laboratory of Quantum Optics and Quantum Optics Devices, Institute of Laser Spectroscopy, Shanxi University, Taiyuan 030006, China; Hao_liping@163.com (L.H.); xym114356966@163.com (Y.X.); Fan_jiabei@163.com (J.F.); ycjiao@sxu.edu.cn (Y.J.); tjia@sxu.edu.cn (S.J.)

² Collaborative Innovation Center of Extreme Optics, Shanxi University, Taiyuan 030006, China

* Correspondence: zhaojm@sxu.edu.cn

Received: 20 March 2019; Accepted: 19 April 2019; Published: 25 April 2019



Abstract: An electromagnetically induced transparency (EIT) of a cascade-three-level atom involving Rydberg level in a room-temperature cell, formed with a cesium $6S_{1/2}$ - $6P_{3/2}$ - $66S_{1/2}$ scheme, is employed to detect the Autler-Townes (AT) splitting resulted with a 15.21-GHz microwave field coupling the $66S_{1/2} \rightarrow 65P_{1/2}$ transition. Microwave field induced AT splitting, f_{AT} , is characterized by the distance of peak-to-peak of an EIT-AT spectrum. The f_{AT} dependence on the microwave Rabi frequency, Ω_{MW} , demonstrates two regions, the strong-coupling linear region, $f_{AT} \approx \Omega_{MW}$ and the weak-coupling nonlinear region, $f_{AT} \lesssim \Omega_{MW}$. The f_{AT} dependencies on the probe and coupling Rabi frequency are also investigated. Using small probe- and coupling-laser, the Rabi frequency is found to enlarge the linear regime and decrease the uncertainty of the microwave field measurements. The measurements agree with the calculations based on a four-level atomic model.

Keywords: Rydberg EIT-AT; cascade four-level atom; nonlinearity effect

1. Introduction

Atom-based measurements are receiving increasing attention, such as time [1], gravity [2] and electromagnetic fields [3–5], due to their invariable level structures that can be used as self-calibrating criteria for measurements of these quantities. Atoms have also been successfully used for magnetometry due to their sensitivity to magnetic field [6,7]. Rydberg atom, highly excited atom with principal quantum number $n > 10$, has a large electric polarizability ($\propto n^7$) and a big microwave-transition dipole moments ($\propto n^2$) [8], which make it a good candidate for measuring external electric fields [9–15]. Rydberg electromagnetically induced transparency (EIT) [16,17], providing a nondestructive detection of Rydberg states, has been investigated in recent years. Rydberg EIT can be used to measure a large dynamic range of the electric fields of electromagnetic radiation, including microwave fields [10–12], millimeter waves [13], static electric fields [14,15] and subwavelength imaging of microwave electric-field distributions [18,19] and field inhomogeneities [20].

Measurement of the microwave field for frequency larger than 1 GHz is mainly based on an Autler-Townes (AT) effect [21] that is induced by the microwave field coupling nearby Rydberg levels [10]. Rydberg-EIT is employed to measure the AT splitting (f_{AT}) that is proportional to the microwave electric field, i.e., $f_{AT} = \Omega_{MW} = \frac{\mu_{MW}E}{\hbar}$, with Ω_{MW} the Rabi frequency of microwave field, μ_{MW} the dipole matrix element microwave field coupled and \hbar reduced Planck constant. The Rydberg EIT-AT spectrum leads to a direct International System of Units (SI) traceable, self-calibration and broadband measurement of microwave electric fields, that has the capability to realize measurements

on a fine spatial resolution. The approach of EIT/AT-based electric-field measurement is recently investigated by several groups around the world [9–13]. However, the AT splitting shows the nonlinear dependence on the coupling Ω_{MW} at a weak electric-field range, which yield a large deviation of the microwave electric-field measurement. Here, we present the measurements of f_{AT} , induced by a 15.21-GHz microwave field coupling the $66S_{1/2}$ - $65P_{1/2}$ Rydberg transition in a cesium room-temperature vapor cell. We investigate the dependences of the f_{AT} on the Ω_{MW} and the coupling (probe) Rabi frequency $\Omega_{c(p)}$. The results are in accord with the theoretical simulation of the density matrix theory.

2. Experimental Setup

A schematic of an experimental setup and relevant Rydberg EIT-AT four-level ladder diagram are shown in Figure 1a,b. A weak probe beam, with $1/e^2$ waist $90\ \mu\text{m}$ and wavelength $\lambda_p = 852\ \text{nm}$, and a strong coupling laser, with $1/e^2$ waist $135\ \mu\text{m}$ and wavelength $\lambda_c = 510\ \text{nm}$, are overlapped and counter-propagated through a room-temperature cylindrical cesium vapor cell. Both length and diameter of the cell are $25\ \text{mm}$. Cesium ground state $|6S_{1/2}F = 4\rangle$, excited state $|6P_{3/2}F' = 5\rangle$, and Rydberg state $|66S_{1/2}\rangle$ consist of a three-level EIT system. The coupling laser couples the transition, $|6P_{3/2}F' = 5\rangle \rightarrow |66S_{1/2}\rangle$. The probe laser is frequency-locked to the transition $|6S_{1/2}F = 4\rangle \rightarrow |6P_{3/2}F' = 5\rangle$ using a polarization spectrum method. The microwave electric field with a frequency $\sim 15.21\ \text{GHz}$ is emitted from an antenna that is placed at a distance of $86\ \text{cm}$ from the vapor cell, see Figure 1a. The microwave field couples the Rydberg transition $|66S_{1/2}\rangle \rightarrow |65P_{1/2}\rangle$, yielding a Rydberg EIT-AT spectrum.

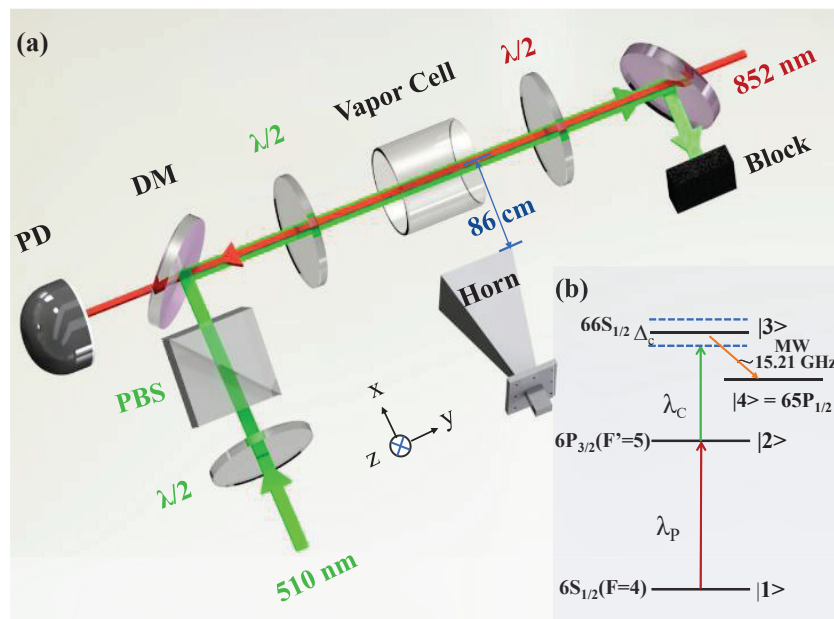


Figure 1. (color online) (a) Sketch of an experimental setup. The coupling, $\lambda_c = 510\ \text{nm}$, and probe, $\lambda_p = 852\ \text{nm}$, lasers counter-propagate through a cesium room-temperature vapor cell along the y -axis. The horn antenna, placed $86\ \text{cm}$ far from the cell (not scaled), emits the microwave electric field with the frequency $\sim 15.21\ \text{GHz}$ coupling Rydberg transition, producing an EIT-AT spectrum. The polarization of the microwave field is set to parallel to the polarization of probe and coupling beams. The probe beam is passed through a dichroic mirror (DM) and is detected with a photodiode detector (PD). PBS: polarized beam splitter; (b) Energy level diagram of cesium cascade four-level system. The probe laser is resonant with the lower transition, $|6S_{1/2}F = 4\rangle \rightarrow |6P_{3/2}F' = 5\rangle$, and the coupling laser is scanned through the Rydberg transitions, $|6P_{3/2}F' = 5\rangle \rightarrow |66S_{1/2}\rangle$. Δ_c is the coupling laser detuning. The applied microwave electric field couples the transition, $|66S_{1/2}\rangle \rightarrow |65P_{1/2}\rangle$, that forms Rydberg EIT-AT spectrum.

The probe and coupling lasers have the same linear polarization along z-axis. The antenna is set such that the polarization of microwave field is paralleled to the laser-beam polarizations. This configuration leads to the two-peak EIT-AT spectral profile. The Rydberg EIT-AT signal is observed by measuring the transmission of the probe laser using a photodiode detector (PD) after a dichroic mirror (DM).

The Rabi frequency of probe (coupling) laser is expressed as, $\Omega_{p(c)} = \frac{\mu_{p(c)}}{\hbar} \sqrt{\frac{2P_{p(c)}}{\pi\omega_{p(c)}^2\epsilon_0}}$, with probe (coupling) laser power $P_{p(c)}$, beam waist $\omega_{p(c)}$, permittivity in vacuum ϵ_0 and light speed c . $\mu_{p(c)}$ is the transition dipole moment corresponding to the probe (coupling) laser coupled transition, which can be calculated accurately [22]. We change the laser Rabi frequency by varying the laser power with a $\lambda/2$ plate that is placed in front of a polarized beam splitter (PBS). Microwave field $E_{MW} = \sqrt{30P_{MW}g/d}$ [23], with P_{MW} power of the microwave source, g gain of the antenna and d distance to the cell. The microwave field is in far-field regime, the distance d is set to 86-cm far from cell, which is larger than the far-field condition, $d_0 = 65$ cm here.

3. Results and Discussion

In Figure 2, we present the measurements of four-time averaged Rydberg EIT-AT spectra with an up level $66S_{1/2}$ Rydberg state, and a 15.21-GHz microwave electric field coupling $|66S_{1/2}\rangle \rightarrow |65P_{1/2}\rangle$ transition. The Rabi frequencies for the probe and coupling beams are $\Omega_p = 2\pi \times 4.00$ MHz and $\Omega_c = 2\pi \times 4.11$ MHz, respectively. The black curve in Figure 2 shows a field-free Rydberg EIT spectrum. EIT linewidth $2\pi \times (5.83 \pm 0.2)$ MHz (close to the natural linewidth $2\pi \times 5.2$ MHz of intermediate state) is extracted by Lorentz fitting to the EIT spectrum. EIT spectrum is calibrated with the hyperfine level $|6P_{3/2}F' = 4\rangle$ Rydberg EIT signal, not shown in here, see ref [14]. It is noted that the observed hyperfine EIT interval of $6P_{3/2}(F' = 5)$ and $(F' = 4)$ is $\eta \times 251$ MHz = 168 MHz, here $\eta = \lambda_p/\lambda_c - 1$ is the Doppler factor. The EIT line splits into two-peak spectra, known as AT effect, when we apply a microwave electric field that couples $|66S_{1/2}\rangle \rightarrow |65P_{1/2}\rangle$ transition. AT splitting, f_{AT} , defined as the peak-to-peak separation of the line pair, is extracted using the multipeak Lorentz fittings to the spectrum, as denoted with the solid lines in Figure 2. The measured f_{AT} are $2\pi \times 12.90$ MHz and $2\pi \times 39.26$ MHz for microwave power of 0.63 mW and 5.01 mW, respectively. The measured AT splitting, f_{AT} , shows increasing with the microwave electric field.

For further investigating the dependence of EIT-AT splitting f_{AT} on the microwave field, we do a series of measurements by varying the microwave power. Figure 3 demonstrates f_{AT} dependence on the microwave Rabi frequency Ω_{MW} with probe $\Omega_p = 2\pi \times 4.00$ MHz and two coupling Rabi frequency $\Omega_{c1} = 2\pi \times 4.11$ MHz (red circles) and $\Omega_{c2} = 2\pi \times 2.06$ MHz (blue squares). It is seen that $f_{AT} \approx \Omega_{MW}$ and linearly increases with microwave at the region $\Omega_{MW} \gtrsim 2\pi \times 17$ MHz, in a strong field region, for both cases. According to $f_{AT} \approx \Omega_{MW}$ and $\Omega_{MW} = \frac{\mu_{MW}E}{\hbar}$, the microwave electric field E can be measured [10]. However, in a weak region, measured f_{AT} is less than Ω_{MW} and denotes a nonlinear dependence, see the inset of Figure 3. The nonlinear behavior is attributed to the EIT effect when probe and coupling fields interact with atoms at a weak-coupling region [24,25].

It is found, from Figure 3's inset, that the nonlinearity of f_{AT} strongly depends on the microwave-free Rydberg EIT condition, i.e., the EIT linewidth. γ_{EIT} is expressed as $(\Omega_c^2 + \Omega_p^2)/\Gamma_{eg}$ with Γ_{eg} the spontaneous decay rate of intermediate state. EIT linewidth depends on the probe and coupling laser Rabi frequency. For the case $\Omega_{c1} = 2\pi \times 4.11$ MHz in the inset of Figure 3, the $\gamma_{EIT} = 2\pi \times 5.83$ MHz, the f_{AT} begins to show the nonlinear effect at $\Omega_{MW} \simeq 2\pi \times 17$ MHz, that is $\sim 3\gamma_{EIT}$, and demonstrate the highly nonlinear behavior at $\Omega_{MW} \lesssim \gamma_{EIT}$. For the smaller coupling Rabi frequency, $\Omega_{c2} = 2\pi \times 2.06$ MHz and $\gamma_{EIT} = 2\pi \times 4.35$ MHz, we see the nonlinear effect appear at $\Omega_{c1} \simeq 2\pi \times 12.0$ MHz ($\sim 3\gamma_{EIT}$). At a weak-field region, the AT peaks are artificially pulled closer together for simultaneously that leads to $f_{AT} < \Omega_{MW}$. The phenomenon about nonlinear dependence are similar with the theoretical simulation in Ref. [12]. At a nonlinear region, $f_{AT} \lesssim \Omega_{MW}$, yielding large uncertainty and prevents the precise measurement of the microwave field.

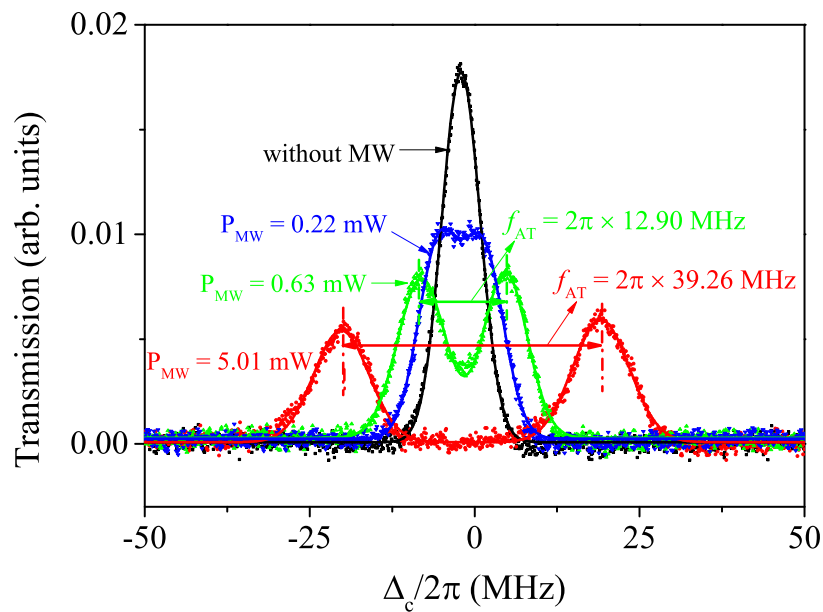


Figure 2. (color online) Measurements of Rydberg EIT-AT spectra as a function of the coupling laser detuning Δ_c with the probe/coupling Rabi frequency $\Omega_p = 2\pi \times 4.00$ MHz and $\Omega_c = 2\pi \times 4.11$ MHz and the indicated microwave power $P = 0.22$ mW (blue), 0.63 mW (green) and 5.01 mW (red). The frequency of microwave field is set to 15.21 GHz coupling Rydberg transition $|66S_{1/2}\rangle \rightarrow |65P_{1/2}\rangle$. The microwave induced AT splitting, f_{AT} , is extracted with the multipole Lorentz fittings to the EIT-AT spectra (solid lines). The microwave-free EIT signal (black) is obtained with $6S_{1/2}$ - $6P_{3/2}$ - $66S_{1/2}$ three-level scheme, corresponding EIT linewidth $\gamma_{EIT} = 2\pi \times (5.83 \pm 0.2)$ MHz.

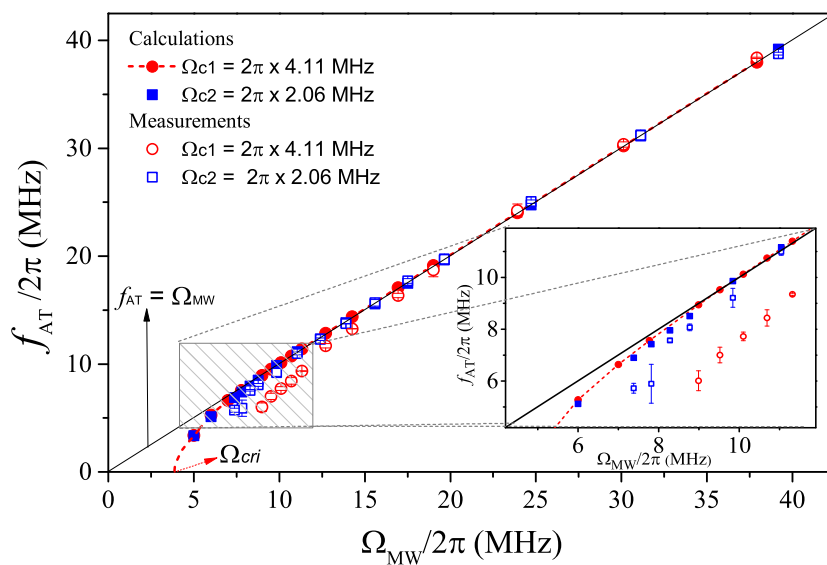


Figure 3. (color online) Measurements (hollow) and calculations (solid) of f_{AT} as a function of microwave Rabi frequency Ω_{MW} for the probe Rabi frequency $\Omega_p = 2\pi \times 4.00$ MHz and two different coupling Rabi frequency $\Omega_{c1} = 2\pi \times 4.11$ MHz (red circles) and $\Omega_{c2} = 2\pi \times 2.06$ MHz (blue squares). f_{AT} shows linear increase as microwave field, and $f_{AT} \approx \Omega_{MW}$ in a strong microwave coupling range, when $\Omega_{MW} \gtrsim 2\pi \times 17$ MHz for the case Ω_{c1} and $\gtrsim 2\pi \times 10$ MHz for the case Ω_{c2} ; whereas $f_{AT} < \Omega_{MW}$, demonstrating the nonlinear dependence on the microwave field. Inset: a room-in of nonlinear region indicated by the gray rectangle. The black thin line indicates the reference $f_{AT} = \Omega_{MW}$.

To explain the experimental results in Figure 3, we numerically solve the master equation,

$$\dot{\rho} = -\frac{i}{\hbar}[H, \rho] + \mathcal{L} \tag{1}$$

where H is the Hamiltonian of the four-level atomic system in Figure 1b, and \mathcal{L} is the Lindblad operator that accounts for the decay processes of the atom, the details of the decay are described in Refs. [12,24].

$$H = \frac{\hbar}{2} \begin{pmatrix} 0 & \Omega_p & 0 & 0 \\ \Omega_p & -2\Delta_p & \Omega_c & 0 \\ 0 & \Omega_c & -2(\Delta_p + \Delta_c) & \Omega_{MW} \\ 0 & 0 & \Omega_{MW} & -2(\Delta_p + \Delta_c + \Delta_{MW}) \end{pmatrix}, \tag{2}$$

where $\Delta_p, \Delta_c, \Delta_{MW}$ are the detunings of the probe laser, couple laser, and the MW field, respectively. Lindblad operator, \mathcal{L} , is denoted as

$$\mathcal{L} = \begin{pmatrix} \Gamma_2\rho_{22} & -\gamma_{12}\rho_{12} & -\gamma_{13}\rho_{13} & -\gamma_{14}\rho_{14} \\ -\gamma_{21}\rho_{21} & \Gamma_3\rho_{33} - \Gamma_2\rho_{22} & -\gamma_{23}\rho_{23} & -\gamma_{24}\rho_{24} \\ -\gamma_{31}\rho_{31} & -\gamma_{32}\rho_{32} & \Gamma_4\rho_{44} - \Gamma_3\rho_{33} & -\gamma_{34}\rho_{34} \\ -\gamma_{41}\rho_{41} & -\gamma_{42}\rho_{42} & -\gamma_{43}\rho_{43} & -\Gamma_4\rho_{44} \end{pmatrix}, \tag{3}$$

where $\gamma_{ij} = (\Gamma_i + \Gamma_j)/2$ and $\Gamma_{i(j)}$ is the spontaneous decay rate. We find the steady-state solution for various values of Ω_c, Ω_p and Ω_{MW} by setting $\dot{\rho} = 0$ and obtain the matrix element ρ_{12} that is proportional to the absorption coefficient of the probe laser [25]. The Beer's absorption coefficient for the probe is $\alpha = 2\pi \frac{Im(\chi)}{\lambda_p}$, with χ the susceptibility of the medium seen by the probe laser. Considering atomic velocity distribution at temperature T , χ is written as $\chi(v)d(v) \propto \rho_{12} N(v)d(v)$, and $N(v)$ is the Maxwellian velocity distribution function at T . In Figure 3, we also present calculated f_{AT} with filled circles (Ω_{c1}) and squares (Ω_{c2}). We note that the calculations show agreement well with measurements at a large Ω_{MW} region for two coupling Rabi frequency cases; whereas at a weak Ω_{MW} region, the calculated f_{AT} display a nonlinear dependence, but measurements for the small Rabi frequency (Ω_{c2}) is closer to the calculations than the large (Ω_{c1}) case. Furthermore, the calculated f_{AT} is almost the same at an interested Ω_{MW} range for two Ω_c cases, this is attributed to the coupling-laser induced EIT line broadening that is not taken into account in our calculations.

To verify the assumption of EIT line broadening, we keep microwave Ω_{MW} fixed and vary the probe/coupling laser Rabi frequency and do a series of measurements of f_{AT} . In Figure 4, we display the f_{AT} dependence on Ω_p in Figure 4a and Ω_c in Figure 4b with $\Omega_{MW} = 2\pi \times 7.61$ MHz (corresponding to $E_{MW} = 0.46$ V/m) and $\Omega_{MW} = 2\pi \times 9.48$ MHz ($E_{MW} = 0.57$ V/m). It is seen that the f_{AT} shows different value as Ω_c or Ω_p varies. For the range Ω_c and Ω_p we used in Figure 4, microwave-free EIT linewidth $\gamma_{EIT} \lesssim 2\pi \times 6.5$ MHz. The f_{AT} is located in the nonlinear region due to microwave $\Omega_{MW} = 2\pi \times 7.61$ MHz (9.48 MHz) that is smaller than $3\gamma_{EIT}$, which result in f_{AT} less than Ω_{MW} . The error bars in Figure 4 display the standard error of four times measurements. The error bar of Figure 4a is less than ± 0.18 for $\Omega_p/2\pi < 4$ MHz, and increases with Ω_p , this is because the large probe Rabi frequency leads to an EIT linewidth that approaches to Ω_{MW} . The f_{AT} fluctuation below $\Omega_p/2\pi = 4$ MHz may due to the inhomogeneous of the microwave field in the cell. In Figure 4b, the error bar decrease with coupling Rabi frequency, which is attributed to the large Ω_c yielding enhanced EIT-AT spectrum. The deviations coming from the nonlinear behavior for the cases in Figures 3 and 4 would result in a measurement uncertainty.

In order to investigate how the probe/coupling laser affect the microwave electric field measurement for f_{AT} at a linear and nonlinear regions, we do the measurements and analysis the field-measurements uncertainty. In Figure 5, we present four-time averaged EIT-AT spectra for the f_{AT} at a linear region with $\Omega_{MW} = 2\pi \times 30.71$ MHz (Figure 5a,b) and a nonlinear region with $\Omega_{MW} = 2\pi \times 7.73$ MHz (Figure 5c-e) and indicated coupling Ω_c . For comparison, we also plot the

calculations based on the four-level model, see solid lines in Figure 5. The microwave Rabi frequency Ω_{MW} used in calculations are same as f_{AT} for linear regime in Figure 5a,b, the calculations reproduce the EIT-AT spectra well. The small difference at shoulder of the AT peak is due to the inhomogeneous of MW field in the cell that yields the AT line broaden [23]. In Figure 5c–e, the microwave Rabi frequency Ω_{MW} in calculations has a tiny difference with the measured f_{AT} . Below we analysis the relative deviation, D_{Err} , that is defined as the ratio $(f_{AT} - \Omega_{MW})/\Omega_{MW}$. In the linear region, the measured $f_{AT} \approx \Omega_{MW}$ and independent of the coupling Rabi frequency. The extracted D_{Err} is -0.52% and 0.88% , see Figure 5a,b, which are smaller than 1%. However, in the nonlinear region, for the same microwave field the measured f_{AT} display different value and varies with the coupling laser Rabi frequency leading to large deviations of field measurements. The resultant uncertainty D_{Err} in Figure 5c–e are -11.38% , 0.52% and 9.31% for $\Omega_c/2\pi = 3.56$ MHz, 2.06 MHz and 1.13 MHz, respectively. The results of Figures 4 and 5 provide experimental evidence for the theoretical simulations in Ref. [12].

From the results of Figures 3–5, it is seen that the f_{AT} shows two regions, the strong microwave Ω_{MW} linear region and the weak field nonlinear region. At the linear region, $f_{AT} \approx \Omega_{MW}$, which can be used to measure precisely the microwave electric field with uncertainty less than 1%, see Figure 5a,b, one orders of magnitude better than the conventional microwave field measurements. At the nonlinear region, f_{AT} strongly depends on the microwave-free EIT linewidth, relying on the probe and coupling laser Rabi frequency. From Figures 3 and 5c–e, the smaller the coupling Ω_c is, the narrower the microwave-free EIT linewidth is and the smaller the f_{AT} can be separated, see Figure 5c,d. However, when the coupling Ω_c is further decreased, the EIT-AT spectrum shows good two-peak profile but with low signal-noise ratio, which also leads to the large measurement uncertainty in Figure 5c. For the electric field measurement using EIT-AT, the narrow EIT linewidth is expected to obtain a large f_{AT} linear region and precise microwave field measurements.

From Figure 3, we note that this nonlinear behavior also leads to a critical value for Ω_{cri} before AT splitting occurs. The critical value corresponds to the minimum splitting that can be detected and is given by the locations where the curves cross the x -axis, Ω_{cri} , see the short-dashed arrow in Figure 3. For $\Omega_{MW} \lesssim \Omega_{cri}$, the microwave electric field cannot be measured with this EIT-AT method. The Ω_{cri} is relative to the EIT linewidth, γ_{EIT} . The narrower the γ_{EIT} is, the smaller Ω_{cri} is. The narrow linewidth EIT spectrum can be obtained with a weak coupling(probe) laser beam (small Rabi frequency). However, this strategy to reduce EIT linewidth has a limitation that is limited by the Doppler broadening. For reducing the EIT linewidth further, it need to lower the temperature of the atomic vapor and using the laser trapped atoms. In other hand, using weak probe(coupling) laser Rabi frequency will increase the background noise and reducing the sensitivity, see Figure 5c.

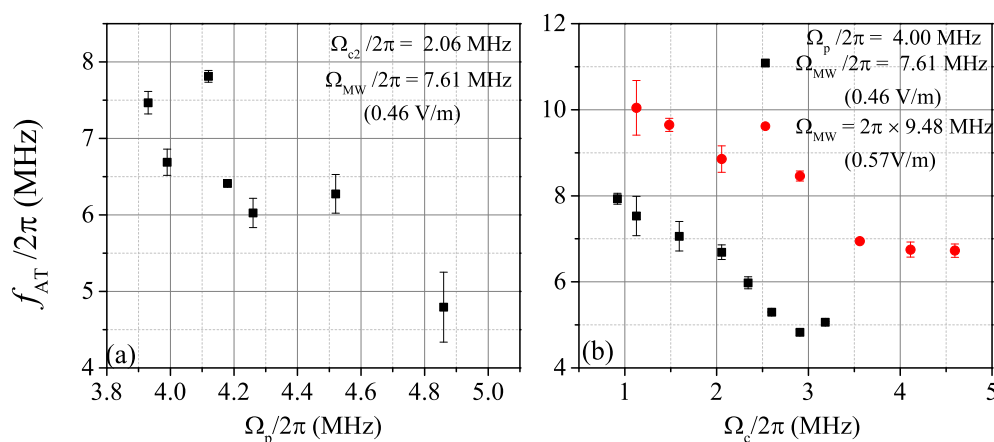


Figure 4. (color online) Measurements of f_{AT} as a function of probe Rabi frequency Ω_p (a) and coupling Rabi frequency Ω_c (b) for fixed microwave electric field $\Omega_{MW}/2\pi = 7.61$ MHz and 9.48 MHz, corresponding to electric field $E = 0.46$ V/m and 0.57 V/m, respectively. The error bars show the standard error of four times measurements.

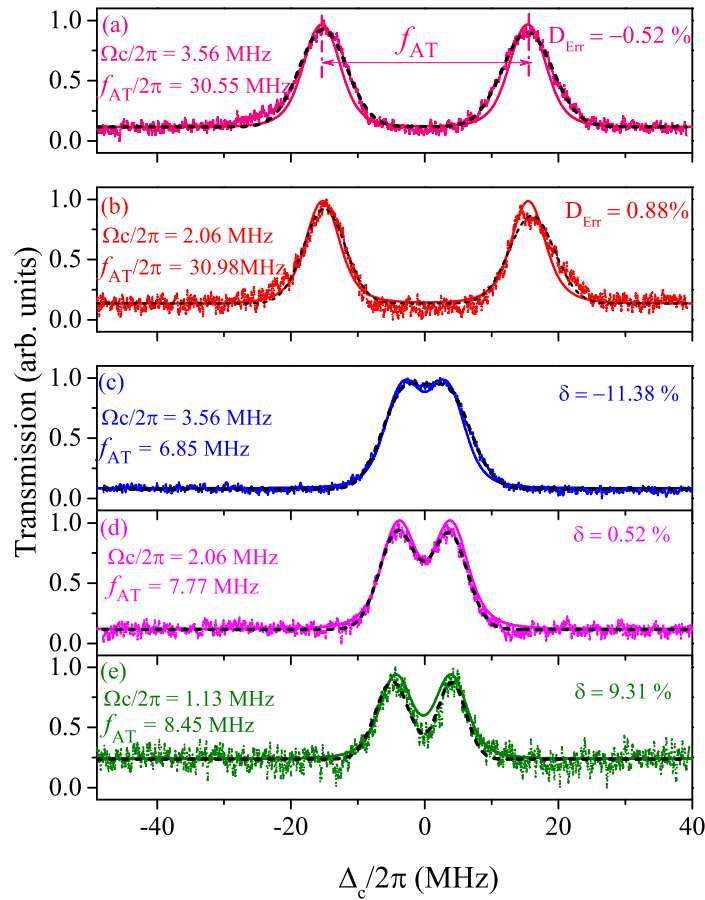


Figure 5. (color online) Measurements (symbols) and calculations (solid lines) of Rydberg EIT-AT spectra as a function of the coupling laser detuning Δ_c and indicated coupling Rabi frequencies for fixed probe $\Omega_p = 2\pi \times 4.00$ MHz and two microwave field $\Omega_{MW} = 2\pi \times 30.71$ MHz (a,b) and $2\pi \times 7.73$ MHz (c–e). The black dashed lines display multipeak Lorentz fittings to the EIT-AT spectra for extracting f_{AT} . The deviation D_{Err} is defined as the ratio $(f_{AT} - \Omega_{MW})/\Omega_{MW}$. In (a,b), f_{AT} locates in the linear region where the measured microwave electric field is independent on the coupling laser, corresponding D_{Err} is smaller than 1%. In (c–e), f_{AT} is in the nonlinear region where measured microwave electric field strongly dependent on the coupling laser Ω_c .

4. Conclusions

In conclusion, we have investigated Rydberg EIT-AT spectra employing cesium ladder four-level system involving Rydberg $|66S_{1/2}\rangle$, where a 15.21-GHz microwave field coupling the transition of $|66S_{1/2}\rangle \rightarrow |65P_{1/2}\rangle$. Microwave induced AT splitting f_{AT} is proportional to coupled Rabi frequency $\Omega_{MW} = \frac{\mu_{MW}E}{\hbar}$, providing a self-calibrated and broadband measurement of microwave electric field [10]. The f_{AT} dependence on Ω_{MW} at a weak microwave field region shows a nonlinear effect, $f_{AT} < \Omega_{MW}$. We find that the nonlinear region depends on the microwave-free EIT linewidth. When $\Omega_{MW} \gtrsim 3\gamma_{EIT}$, the measured f_{AT} displays a good linear behavior, the uncertainty of the measured microwave field is less than 1%, while $\Omega_{MW} \lesssim 3\gamma_{EIT}$, f_{AT} enter the nonlinear region, yielding the large measurement uncertainty using this technology. When $\Omega_{MW} \lesssim \gamma_{EIT}$, it shows a highly nonlinear effect, corresponding uncertainty even up to 40%. Figures 4 and 5 demonstrate that using the weak probe and coupling laser beams, forming the narrow linewidth EIT spectrum, can enlarge the linear region and decrease the measurement uncertainty. The narrow linewidth EIT spectrum also can be obtained with a three-photon EIT scheme [26]. To observe a narrow EIT linewidth, one must decrease the probe and coupling laser power. This will increase the background noise as in Figure 5c. We need to balance the linewidth and spectrum sensitivity in experiments. It is noted that this kind of nonlinear

presented in this work and Ref. [12] is inevitable result of the quantum effect, when the Ω_{MW} decrease to the critical value, the system become the quantum interference region, as discussed in our previous work [24]. In future work, the modulation and demodulation technique will be used to improve the Rydberg-atom-based field measurements.

Author Contributions: Conceptualization, J.Z., Y.J. and L.H.; investigation, J.Z., Y.J. and L.H.; software, Y.J. and Y.X.; validation, L.H., Y.X. and J.F.; formal analysis, L.H., Y.X. and J.F.; Writing—original draft, L.H.; writing—review and editing, J.Z.; project administration, S.J., J.Z. and Y.J.; funding acquisition, S.J., J.Z. and Y.J.

Funding: The work was supported by the National Key R&D Program of China (Grant No. 2017YFA0304203), the National Natural Science Foundation of China (Grants No. 61675123, No. 61775124 and 11804202), Changjiang Scholars and Innovative Research Team in University of Ministry of Education of China (Grant No. IRT13076), and the State Key Program of National Natural Science of China (Grant No. 11434007 and 61835007).

Conflicts of Interest: The authors declare no conflict of interest.

References

1. Martin, M.J.; Bishof, M.; Swallows, M.D.; Zhang, X.; Benko, C.; von-Stecher, J.; Gorshkov, A.V.; Rey, A.M.; Ye, J. A quantum many-body spin system in an optical lattice clock. *Science* **2013**, *341*, 632–636. [[CrossRef](#)]
2. Biedermann, G.W.; Wu, X.; Deslauriers, L.; Roy, S.; Mahadeswaraswamy, C.; Kasevich, M.A. Testing gravity with cold-atom interferometers. *Phys. Rev. A* **2015**, *91*, 033629. [[CrossRef](#)]
3. Savukov, I.M.; Seltzer, S.J.; Romalis, M.V.; Sauer, K.L. Tunable atomic magnetometer for detection of radio-frequency magnetic fields. *Phys. Rev. Lett.* **2005**, *95*, 063004. [[CrossRef](#)]
4. Horsley, A.; Du, G.-X.; Pellaton, M.; Affolderbach, C.; Mileti, G.; Treutlein, P. Imaging of relaxation times and microwave field strength in a microfabricated vapor cell. *Phys. Rev. A* **2013**, *88*, 063407. [[CrossRef](#)]
5. Horsley, A.; Du, G.-X.; Treutlein, P. Widefield microwave imaging in alkali vapor cells with sub-100 μm resolution. *New J. Phys.* **2015**, *17*, 112002. [[CrossRef](#)]
6. Patton, B.; Versolato, O.O.; Hovde, D.C.; Corsini, E.; Higbie, J.M.; Budker, D. A remotely interrogated all-optical ^{87}Rb magnetometer. *Appl. Phys. Lett.* **2012**, *101*, 083502. [[CrossRef](#)]
7. Budker, D.; Romalis, M. Optical magnetometry. *Nat Phys.* **2007**, *3*, 227–234. [[CrossRef](#)]
8. Gallagher, T.F. *Rydberg Atoms*; Cambridge University Press: New York, NY, USA, 1994.
9. Holloway, C.L.; Gordon, J.A.; Jefferts, S.; Schwarzkopf, A.; Anderson, D.A.; Miller, S.A.; Thaicharoen, N.; Raithel, G. Broadband Rydberg Atom-Based Electric-Field Probe for SI-Traceable, Self-Calibrated Measurements. *IEEE Trans. Antennas Propag.* **2014**, *62*, 6169–6182. [[CrossRef](#)]
10. Sedlacek, J.A.; Schwettmann, A.; Kübler, H.; Löw, R.; Pfau, T.; Shaffer, J.P. Microwave electrometry with Rydberg atoms in a vapour cell using bright atomic resonances. *Nat. Phys.* **2012**, *8*, 819–824. [[CrossRef](#)]
11. Fan, H.Q.; Kumar, S.; Sedlacek, J.; Kübler, H.; Karimkashi, S.; Shaffer, J.P. Atom based RF electric field sensing. *J. Phys. B At. Mol. Opt. Phys.* **2015**, *48*, 202001. [[CrossRef](#)]
12. Holloway, C.L.; Simons, M.T.; Gordon, J.A.; Dienstfrey, A.; Anderson, D.A.; Raithel, G. Electric field metrology for SI traceability: Systematic measurement uncertainties in electromagnetically induced transparency in atomic vapor. *J. Appl. Phys.* **2017**, *121*, 233106. [[CrossRef](#)]
13. Gordon, J.A.; Holloway, C.L.; Schwarzkopf, A.; Anderson, D.A.; Miller, S.; Thaicharoen, N.; Raithel, G. Millimeter wave detection via Autler-Townes splitting in rubidium Rydberg atoms. *Appl. Phys. Lett.* **2014**, *105*, 024104. [[CrossRef](#)]
14. Jiao, Y.C.; Han, X.X.; Yang, Z.W.; Li, J.K.; Raithel, G.; Zhao, J.M.; Jia, S.T. Spectroscopy of cesium Rydberg atoms in strong radio-frequency fields. *Phys. Rev. A* **2016**, *94*, 023832. [[CrossRef](#)]
15. Jiao, Y.C.; Hao, L.P.; Han, X.X.; Bai, S.Y.; Raithel, G.; Zhao, J.M.; Jia, S.T. Atom-based radio-frequency field calibration and polarization measurement using cesium nD_J Floquet States. *Phys. Rev. Appl.* **2017**, *8*, 014028. [[CrossRef](#)]
16. Fleischhauer, M.; Imamoglu, A.; Marangos, J.P. Electromagnetically induced transparency: Optics in coherent media. *Rev. Mod. Phys.* **2005**, *77*, 633–673. [[CrossRef](#)]
17. Mohapatra, A.K.; Jackson, T.R.; Adams, C.S. Coherent optical detection of highly excited Rydberg states using electromagnetically induced transparency. *Phys. Rev. Lett.* **2007**, *98*, 113003. [[CrossRef](#)]
18. Fan, H.Q.; Kumar, S.; Daschner, R.; Kübler, H.; Shaffer, J.P. Sub-wavelength microwave electric field imaging using Rydberg atoms inside atomic vapor cells. *Opt. Lett.* **2014**, *39*, 3030–3033. [[CrossRef](#)]

19. Holloway, C.L.; Gordon, J.A.; Schwarzkopf, A.; Anderson, D.A.; Miller, S.A.; Thaicharoen, N.; Raithel, G. Sub-wavelength imaging and field mapping via electromagnetically induced transparency and Autler-Townes splitting in Rydberg atoms. *Appl. Phys. Lett.* **2014**, *104*, 244102. [[CrossRef](#)]
20. Fan, H.Q.; Kumar, S.; Sheng, J.T.; Shaffer, J.P.; Holloway, C.L.; Gordon, J.A. Effect of vapor-cell geometry on Rydberg-atom-based measurements of radio-frequency electric fields. *Phys. Rev. Appl.* **2015**, *4*, 044015. [[CrossRef](#)]
21. Autler, S.H.; Townes, C.H. Stark effect in rapidly varying fields. *Phys. Rev.* **1955**, *100*, 703–722. [[CrossRef](#)]
22. Simons, M.T.; Gordon, J.A.; Holloway, C.L. Simultaneous use of Cs and Rb Rydberg atoms for dipole moment assessment and RF electric field measurements via electromagnetically induced transparency. *J. Appl. Phys.* **2016**, *120*, 123103. [[CrossRef](#)]
23. Fan, J.B.; Jiao, Y.C.; Hao, L.P.; Xue, Y.M.; Zhao, J.M.; Jia, S.T. Microwave electromagnetically induced transparency and Autler-Townes spectrum of cesium Rydberg atom. *Acta Phys. Sin.* **2018**, *67*, 093201.
24. Hao, L.P.; Jiao, Y.C.; Xue, Y.M.; Han, X.X.; Bai, S.Y.; Zhao, J.M.; Raithel, G. Transition from electromagnetically induced transparency to Autler-Townes splitting in cold cesium atoms. *New J. Phys.* **2018**, *20*, 073024. [[CrossRef](#)]
25. Scully, M.O.; Zubairy, M.S. *Quantum Optics*; Cambridge University Press: Cambridge, UK, 1997.
26. Kumar, S.; Fan, H.Q.; Kübler, H.; Sheng, J.T.; Shaffer, J.P. Atom-based sensing of weak radio frequency electric fields using homodyne readout. *Sci. Rep.* **2017**, *7*, 42981. [[CrossRef](#)] [[PubMed](#)]



© 2019 by the authors. Licensee MDPI, Basel, Switzerland. This article is an open access article distributed under the terms and conditions of the Creative Commons Attribution (CC BY) license (<http://creativecommons.org/licenses/by/4.0/>).